Seasonal and Interannual Variability in Temperature of the Upper Layer of the Northwest Pacific, 1964–1983

HEUNG-JAE LIE

Korea Ocean Research & Development Institute, Ansan, Republic of Korea

MASAHIRO ENDOH

Meteorological Research Institute, Tsukuba, Japan

(Manuscript received 22 January 1990, in final form 19 September 1990)

ABSTRACT

Available BT data in the northwest Pacific were analyzed to reveal seasonal and interannual variability in thermal structure of the upper 400 m layer in the northwest Pacific. Bimonthly temperature averaged over a 2° × 2° square data in the area within 0°–44°N, 120°E–180° were interpolated to a spatially uniform data grid by combination of the Laplace and spline methods.

Temporal variability of sea surface temperature (SST) is the largest in the seasonal change due to surface heating (July–October) and winter cooling (January–April). The variability at deeper layers below 100 m is primarily interannual in nature. The climatological seasonal cycle of the variation of SST shows that heating and cooling of the surface water start from the western tropical boundary area, extending towards the east and north, and that a certain time lag exists between SST and temperature at a deeper layer. The seasonal change of temperature in the upper layer in the midlatitudes between 15° and 35°N might be explained by the seasonal variation of the thermocline depth, induced by the seasonal change of the wind forcing over the study area.

Horizontal maps of interannual root mean square deviation of temperature, which is the largest at 200 m in the upper 400 m, show a zonal minimum between 15° and 35°N and large interannual variability in the tropical area and high latitudes. Most of the high variability in the tropical area can be explained by the first complex empirical orthogonal function (CEOF) which varies in time with a period of 3–4 years. The CEOF analysis also showed that variability in the tropical area propagates to the northwest with a phase speed of order of 10 cm s^{-1}, which might correspond to the first baroclinic Rossby wave with approximate wavelength of 16 000 km.

1. Introduction

This study is an investigation into seasonal and interannual variability of the thermal structure of the upper 400 m ocean in the northwest Pacific (equator–44°N, 120°E–180°) during the period 1964–83 (Fig. 1).

Several authors have studied interannual variability in sea surface temperature (SST) or in heat content (or vertically average temperature) of the upper ocean in the North Pacific, in relation to El Niño–Southern Oscillation (ENSO) events (e.g., Weare et al. 1976; Davis 1976; White et al. 1985a,b; Hanawa et al. 1988). A major finding of the previous studies is the appearance of a positive anomaly of heat content in the onset phase of ENSO and of negative anomaly during the mature phase in the tropical northwest Pacific. White and Hasunuma (1980) demonstrated that the thermal structure of the upper ocean in midlatitudes of the northwest Pacific fluctuated out of phase with ENSO events in the tropical area.

Although many authors have extensively studied SST or heat content, most of them analyzed data collected for a few years to describe ENSO signals in the tropical area. There are few studies on the overall pattern of seasonal and interannual variabilities in the whole northwest Pacific, which is the main interest of the present study. Concerning the variability of temperature, two questions can be posed as follows: 1) what are major differences in pattern and magnitude between variabilities of SST and temperature at a deeper layer and 2) what is the synoptic pattern of variability in temperature over the whole northwest Pacific? To answer the questions, we examined long-term variability in temperature at various depths of the upper layer by mapping spatial patterns of long-term mean values and standard deviation (section 3), seasonal cycle of temperature variation in terms of amplitude and phase (sections 4 and 5), and interannual variability with periods longer than 1 year (sections 6 and 7).

Corresponding author address: Dr. Heung-Jae Lie, Korea Ocean Research and Development Institute, Ansan, P.O. Box 29, Seoul 425-600, Korea.

2. Data and processing

Data used for the study are temperature–depth observations collected from expendable and mechanical bathythermographs (BT) for a twenty year period 1964–83 in the northwest Pacific. The data were compiled by the Japanese Oceanographic Data Center and the Japanese Far Seas Fisheries. The dataset of the Far Seas Fisheries spanned over part of the period 1975–83 and covered mainly the tropical and equatorial area.

The observed dataset was first quality controlled. The quality control procedure consisted of elimination of spurious values and removal of insufficient observations with temperature data only at one depth. About 200 000 observations were reduced to 133 000 profiles after the quality control, mostly due to coding error and insufficient observations. Figure 1 displays the spatial distribution of the quality-controlled data. The distribution is relatively uniform in space except in the equatorial area where the data are relatively sparse. Maps of the monthly observations also indicate less data north of 40°N during winter (November to February), probably due to high sea states in high latitudes of the study area which may have reduced ship accessibility in winter.

The second step of data processing was preparation of a bimonthly sequential gridded dataset for the 20-year period. In the study area, decorrelation time scales were found to be about three months (White and Bernstein 1979), and space decorrelation scales were reported to be larger than ~100 km (White et al. 1985a). Bimonths considered are January–February through November–December. On the uniform of 2° latitude × 2° longitude grid, the study area is covered by 567 grid points. Data were sorted by grid box and then passed through a test of three times standard deviation to remove unreliable data: temperature data beyond $T_{i,j} \pm 3$ SD were discarded, where $T_{i,j}$ is the mean temperature at the ith grid and the jth bimonth, and SD is the corresponding standard deviation. A bi-

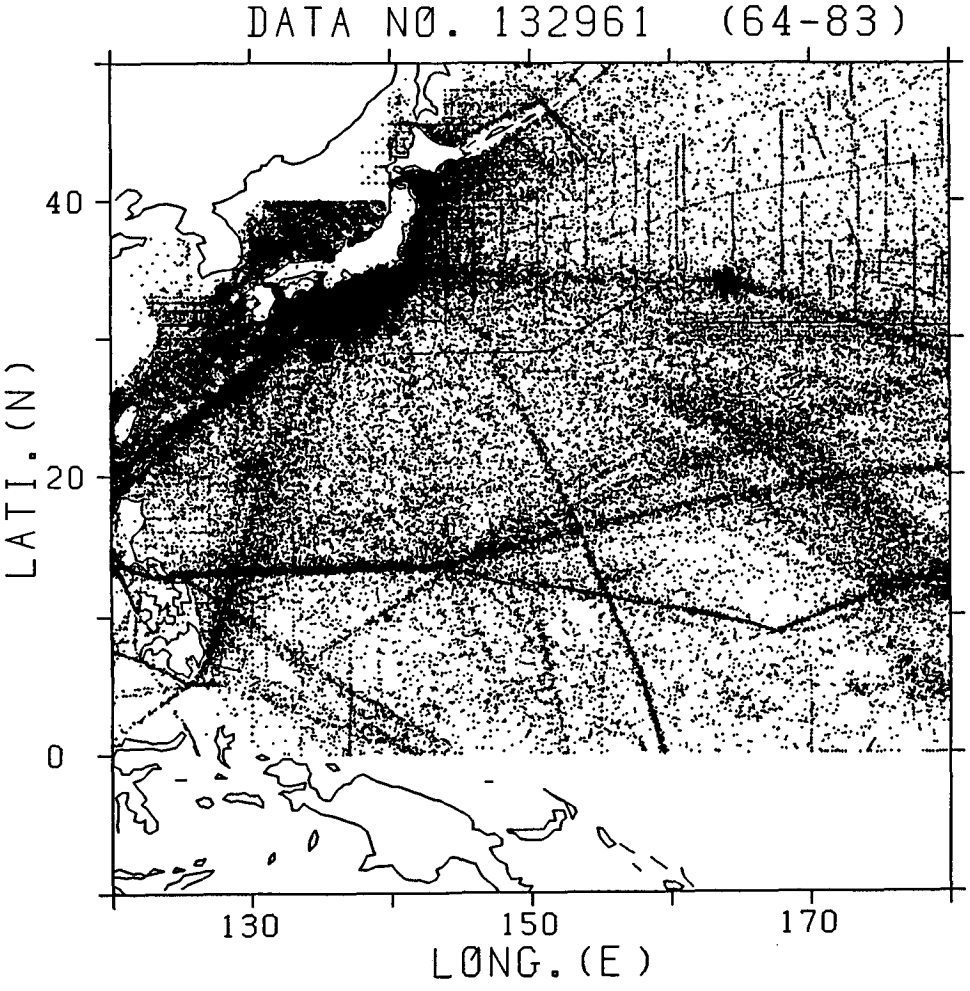

FIG. 1. Distribution map of bathythermograph observations in the western North Pacific during 1964–1983 after the first quality control.

monthly sequential gridded dataset was obtained by averaging all bimonthly data within a grid box, which is hereafter called observed sequential data.

The third step of data processing is preparation of an interpolated dataset for analysis purpose. The observed sequential bimonthly data were spatially interpolated using a combination of the Laplace and spline methods such as:

$$\nabla^2 F(x, y) - \alpha \left(\frac{\partial^4}{\partial x^4} + \frac{\partial^4}{\partial y^4} \right) F(x, y) = 0. \quad (1)$$

In (1), α is an arbitrary constant to be chosen, connecting Laplace and spline methods, i.e., $\alpha = 0$ for Laplace interpolation and $\alpha =$ infinity for spline one. Equation (1) can be estimated within an error $O(h^2)$ by a finite difference method (Davis and Polonsky 1970) for the grid space of h. A missing value at a grid is filled in by a value interpolated by a combination of eight neighboring values located in zonal and meridional directions. Missing values, within five grid spaces distant from the grid where the temperature is observed, are interpolated. The coefficient is taken to be 0.125.

3. Climatological maps of long-term mean temperature

Figures 2 and 3 present climatological maps of the long-term mean temperature and root mean square deviation (RMSD) of temperature at the sea surface, 200 m, and 400 m, calculated from the interpolated sequential dataset. The synoptic patterns of the long-term mean at 200 m are slightly different from those based on the observed sequential data in the equatorial area south of 10°N, where temperature changes sharply in the meridional direction. The difference is mostly due to low density of observations (less than 20% of the total 120 bimonths).

The spatial patterns of the long-term mean and RMSD of sea surface temperature (SST) are very similar to those estimated from a dataset covering longer period (Nagasaka 1983). SST decreases monotonically northward with zonal distribution of isotherms, whereas RMSD increases with latitude. The RMSD is less than 2°C south of 20°N, but greater than 3°C north of 30°N. The northwest Pacific current system is not clearly seen on the mean SST.

The long-term mean temperature at 200 m resembles, in general, the climatological pattern drawn from the dataset prepared by Levitus (1982; redrawn by Shuto 1989) with a small discrepancy in the narrow equatorial band. The mean temperature provides an evidence for the existence of the North Equatorial Current near 12°N and the Kuroshio Extension around 35°N. The Kuroshio and its countercurrent south of Japan are marked by large gradient of temperature. The RMSD at 200 m is radically different in pattern from RMSDs at 0 and 400 m. There is a minimum in the zonal area between 20° and 30°N with values less than 1°C. The high RMSD in the tropical area seems to be associated partly with seasonal change of the Equatorial Current system and mostly with large interannual variations, which will be described in section 6.

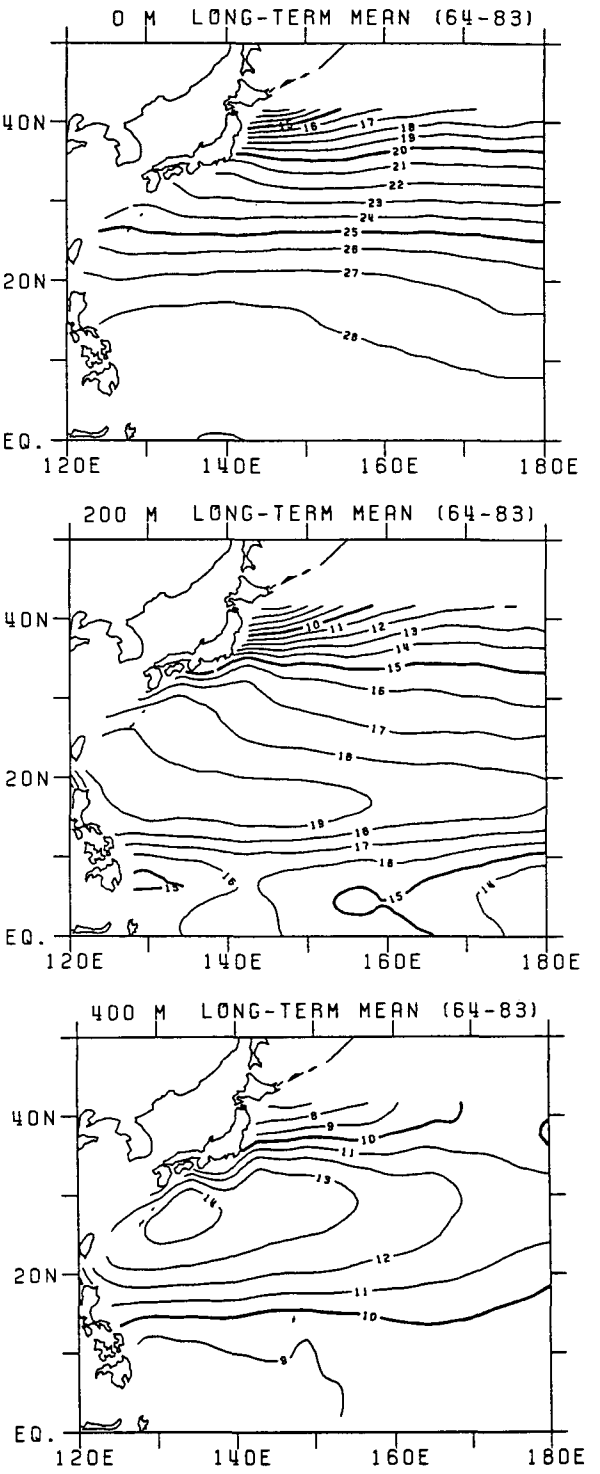

FIG. 2. Long-term annual mean temperature at the sea surface, 200 m, and 400 m.

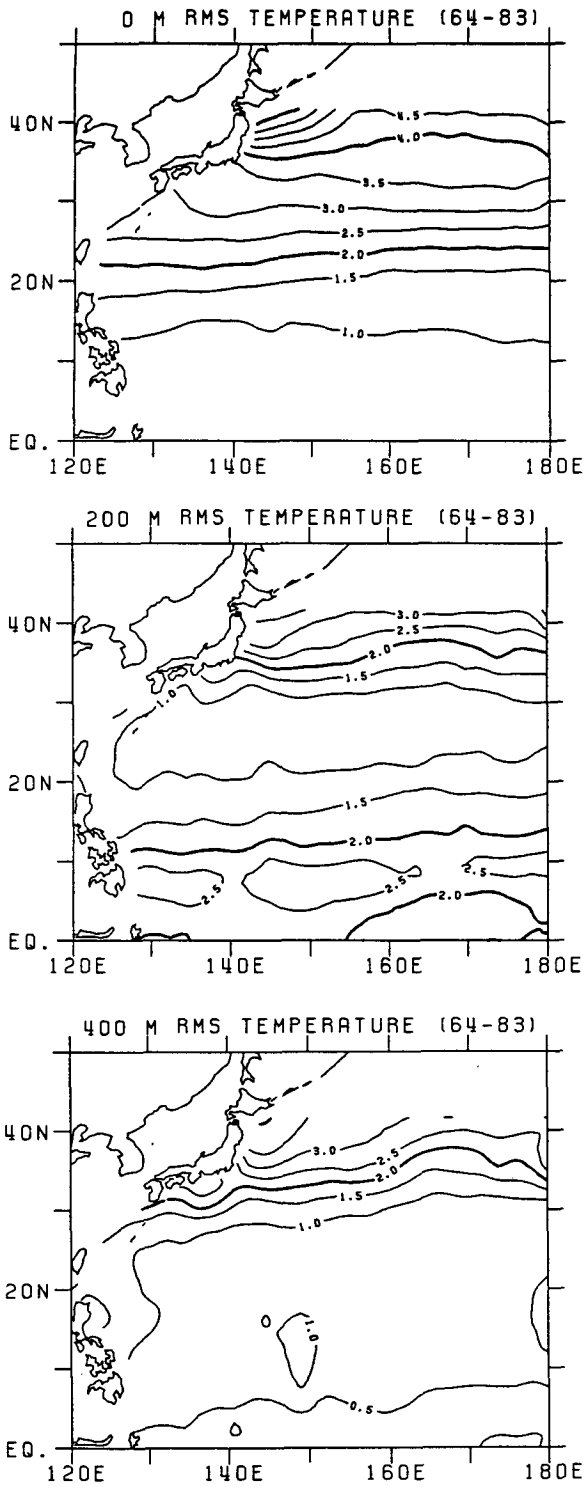

FIG. 3. Root-mean-square temperature of bimonthly temperature at the sea surface, 200 m, and 400 m.

The mean temperature at the depth of 400 m clearly displays the existence of a subtropical anticyclonic circulation between 15° and 35°N. The center of the circulation seems to be located south of the Japanese islands, as identified by the 14°C isotherm. The Equatorial Current, as evidenced by equatorward thermal gradients, is not seen at the 400 m depth. The extension of low RMSD less than 2°C to the south represents a weakening of the Equatorial Current at this depth.

4. Seasonal cycle of temperature variation

The heat content in the surface layer changes seasonally in response to summer heating and winter cooling, and also to the changes of mechanical wind forcing. In order to estimate the contribution of seasonal variation of temperature to the total variance, long-term bimonthly mean temperature distribution and climatological seasonal cycle (one year period) of temperature variation are examined in this section.

Figure 4 presents long-term bimonthly mean temperature at the sea surface. For convenience, the long-term mean is subtracted out, so that the numerical values in Fig. 4 are deviation of bimonthly mean from the long-term annual mean. SST in the two bimonths January–February and March–April is below the annual mean over the whole area and its deviation increases with latitude, being larger than 3°C north of 30°N. In contrast, SST in July–August and September–October is above the annual mean by nearly the same magnitude as that during the cold period. Thus, the annual range of seasonal change in SST becomes more important toward the north, exceeding 8°C north of 35°N. In May–June, a positive local maximum appears in the western tropical area, while SST in midlatitudes is still below the long-term mean, but at the same time a local minimum in the same area during November–December represents the start of cooling in the western boundary region.

The bimonthly mean at 200 m in Fig. 5 is different, compared with the SST distribution. The deviation is positive south of 32°N in March–April but changes sign in September–October when SST is highest, except in the western boundary region. The deviation in high latitudes is maximum in November–December but minimum in July–August, which is opposite to SST. The spatial pattern of bimonthly mean at 400 m is similar to that at 200 m, having a smaller deviation in high latitudes and the tropical area.

Long-term bimonthly mean temperature varies greatly with season and its spatial pattern varies with water depth as we have seen above. To examine more quantitatively the seasonal cycle of variation, its amplitude and phase (one year periodicity) were calculated by a harmonic analysis (Fig. 6). The phase in Fig. 6, measured in degrees, corresponds to the number of days counted from the first of January, when the highest temperature occurs at a given depth.

The spatial patterns of amplitude and phase of the seasonal cycle of SST are in excellent agreement with those calculated by Levitus (1987) from the dataset of

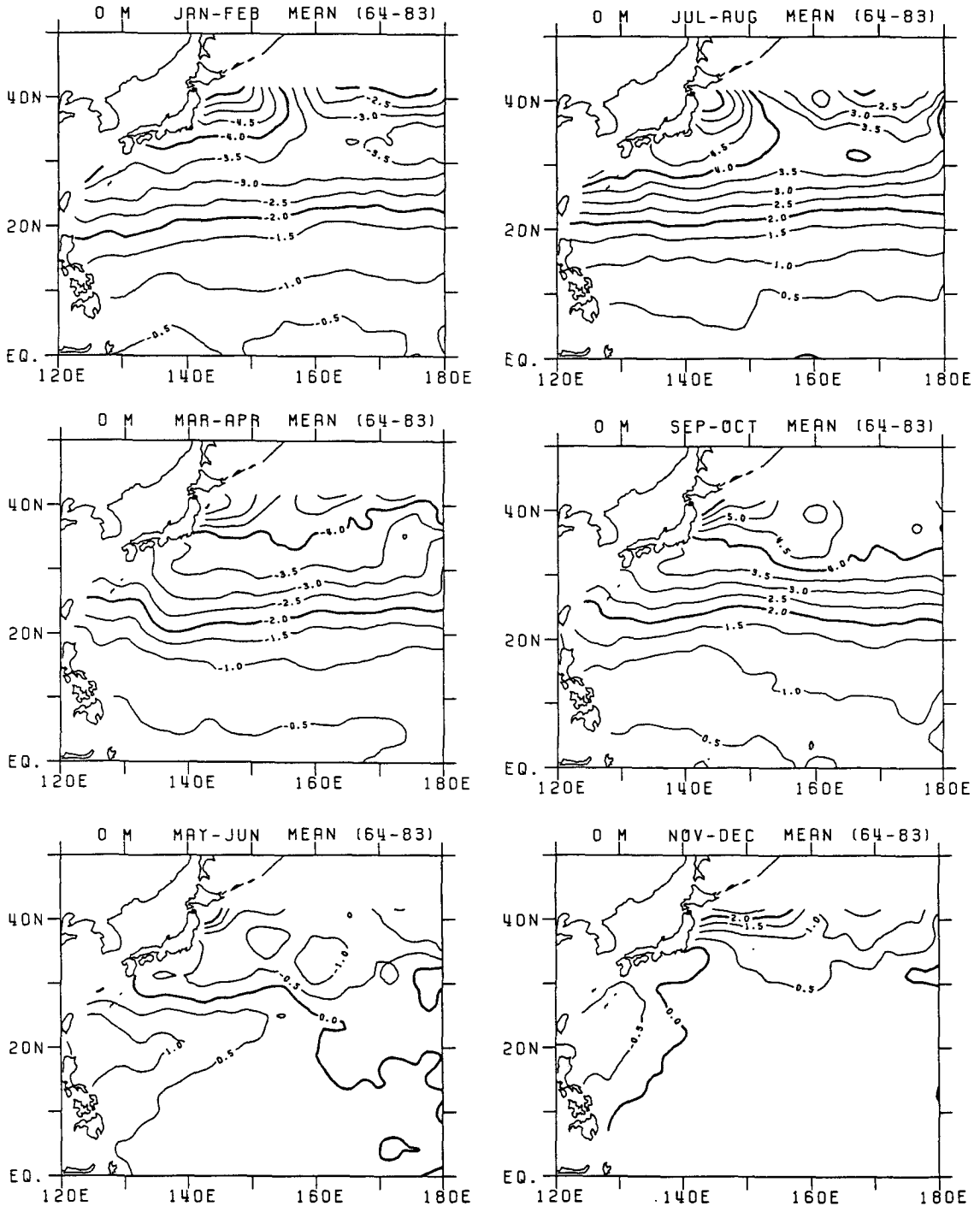

FIG. 4. Long-term bimonthly mean temperature at the sea surface with the long-term mean removed.

the National Oceanographic Data Center and the Comprehensive Ocean–Atmosphere Data Set. The amplitude of the seasonal cycle of SST increases with latitude, showing a zonal distribution as in the cases of SST and RMSD. Large amplitude greater than 5°C, is located just north of the beginning of the Kuroshio Extension. A maximum in amplitude reaching approximately 7°C is found off the east coast of Japan around 40°N. The variance due to the seasonal cycle is given by $A^2/2$, where A is the amplitude. The seasonal cycle of SST variation in Fig. 6 thus explains more than 70% of the total variance (square of the RMSD in Fig. 3). The highest SST in the seasonal cycle occurs in mid-August to early September and the

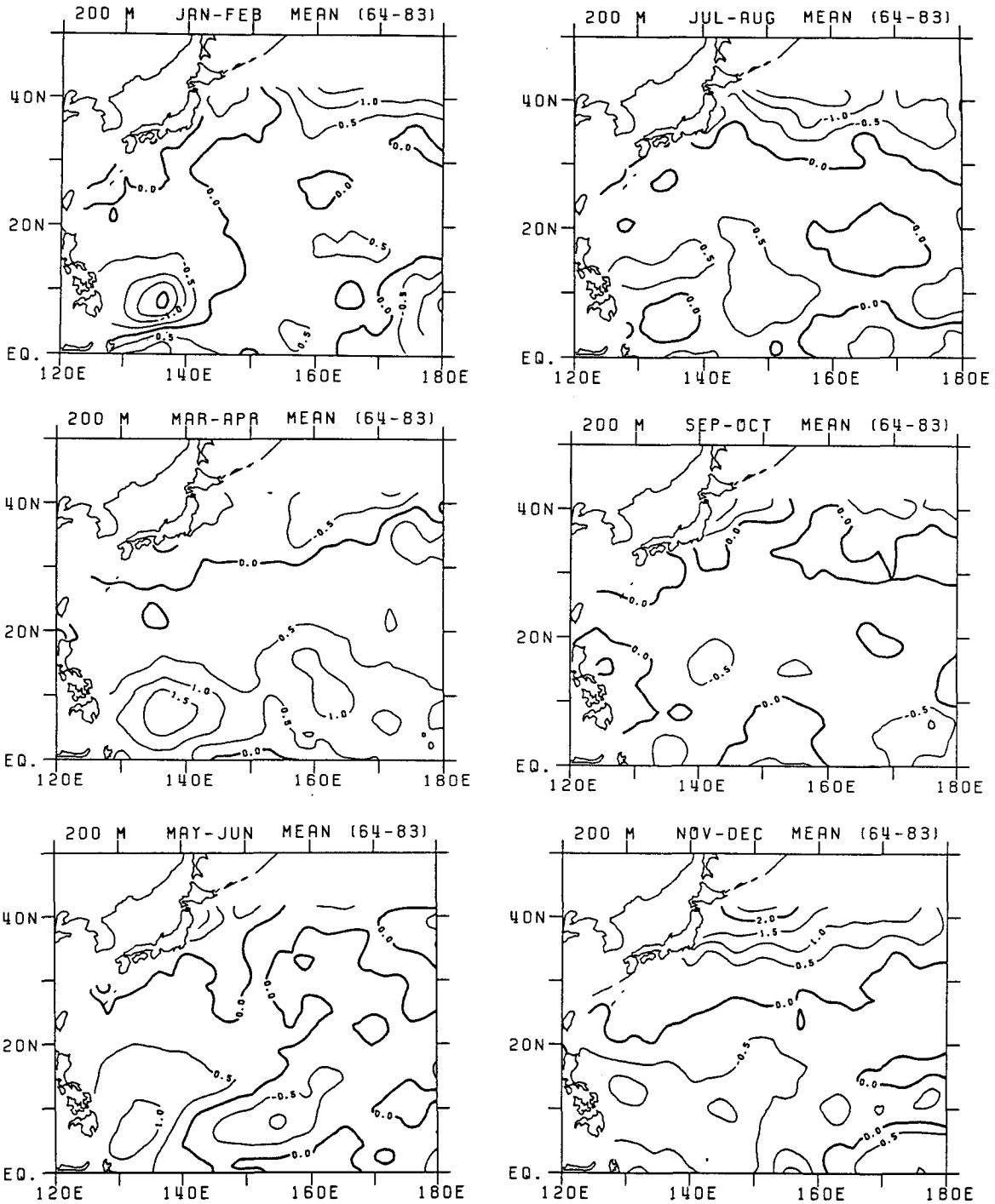

FIG. 5. Long-term bimonthly mean temperature at the depth of 200 m with the long-term mean removed.

phase in the western tropical area leads that over the rest of the area as mentioned previously.

At 200 m, the amplitude of seasonal cycle is zonally minimum in the area between 20° and 35°N with a value less than 0.25, and it becomes more important in lower and higher latitudes. The phase pattern is divided into two types by an axis extending from 28°N; 120°E toward 35°N; 170°E. Phase south of the axis leads that north of the axis by approximately 180 degrees, that is, out of phase. The phase at 400 m is similar in pattern to that at 200 m, but the amplitude in low latitudes is decreased. The larger amplitude at 200 m

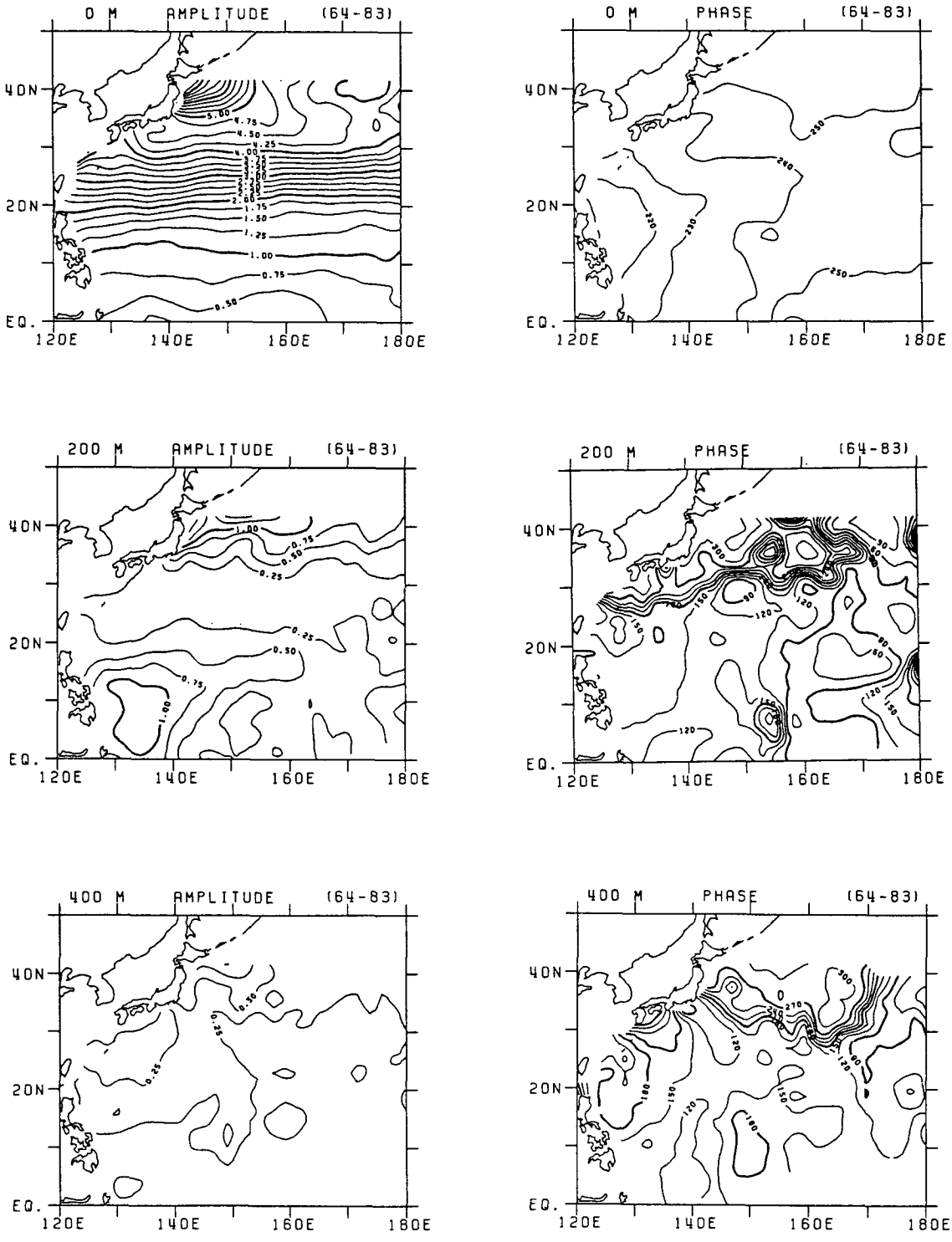

FIG. 6. Amplitude and phase of the seasonal cycle of variation in temperature (one year periodicity) obtained from the bimonthly temperature sequences. The phase corresponds to number of days from the first of January when the highest temperature is recorded.

in the equatorial area, as compared with SST and temperature at 400 m, represents the existence of important seasonal variability in the Equatorial Current area.

5. Comparison of seasonal change of thermocline depth between model and observation

A change in thermocline depth is considered to be an integrated response to local wind stress curl field (Veronis and Stommel 1956). Therefore it could be due to either local or remote forcing. White (1978) compared the observed seasonal change of thermocline depth with the results based on Veronis and Stommel's model. He concluded that the simple two-layer model could not account for the observed amplitude of the seasonal cycle. Although the phase given in Fig. 6 generally resembles that in Fig. 2 of White (1978), the spatial pattern of amplitude is different; in White's work a zonal minimum in amplitude at 200 m does not exist and the amplitude is much larger at 20°–30°N than that of the present study.

Yoshioka and Yoon (1989, called YY hereafter) recently computed seasonal variation of the thermocline depth in the North Pacific using a two-layer quasi-geostrophic model driven by a wind field. The wind field is that prepared by Kutsuwada and Teramoto (1987). According to YY (Fig. 7), the amplitude and phase of the seasonal cycle are zonally distributed and the variation north of 32°N is out of phase with that south of 32°N in the northwest Pacific. It was also found that in the area between 20° and 40°N, the thermocline depth south (north) of 33°N is shallowest (deepest) in May–June, and deepest (shallowest) in November–December. The model results in midlatitudes agree very well with the see-saw–like pattern of the seasonal cycle of temperature at 200 m shown in Fig. 6.

A quantitative comparison of the amplitude of the seasonal cycle of the thermocline depth is made along a longitudinal line at 160°E between the results of YY and the seasonal cycle of isotherm displacement based on the observations. The amplitude of the seasonal cycle of isotherm displacement is that of seasonal vertical

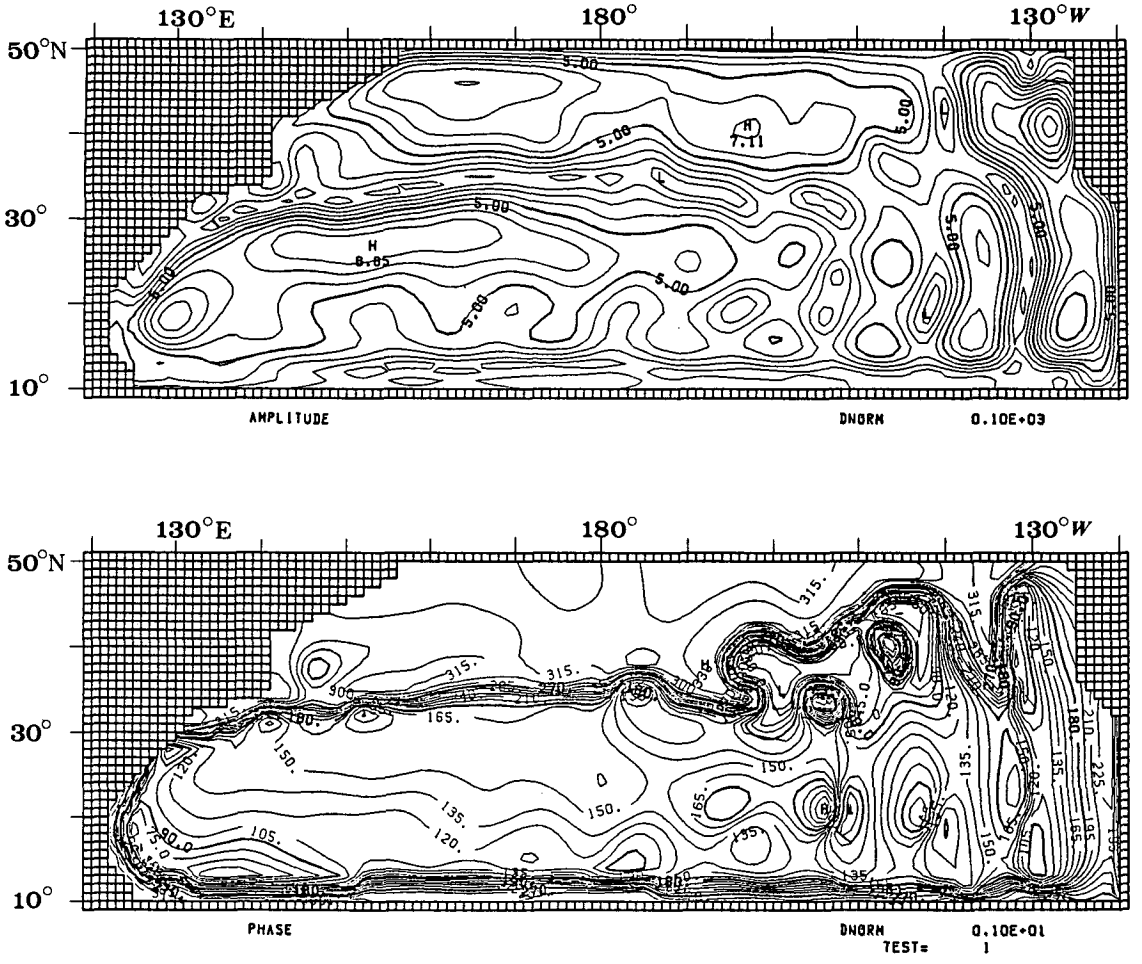

FIG. 7. Amplitude and phase of the seasonal cycle of variation of the thermocline depth in a two-layer wind driven model (after Yoshioka and Yoon 1989). The model basin is 4500 m deep and the interface is located at 300 m. The amplitude is in meters and phase in degrees corresponding to number of days from the first of January when the amplitude is the highest.

height estimated with the amplitude of the seasonal cycle of temperature at 200 and 400 m in Fig. 6 and the long-term mean vertical profiles of temperature along the line, prepared by Shuto (1989). The long-term mean vertical profiles are drawn from the Levitus dataset. Figure 8 displays the model results in the cases of two interface depths of 300 and 600 m, and also the observed amplitude of isotherm displacement at 200 and 400 m. The model amplitude is spatially uniform and less than 8 m with a local maximum around 28°N. There is a very slight difference in amplitude between the two interfaces of 300 and 600 m. However, the observed vertical displacement of isotherms at the two depths, locally minimum around 25°N, increases toward higher and lower latitudes. The large discrepancy between the model and observations north of 32°N and south of 15°N is mostly due to the model limitation. Weak vertical stratification in the high latitudes and the strong thermocline in the tropical area cannot be properly resolved in the two layer model with a uniform mean depth of 300 or 600 m. The disagreement of the observed displacement between 200 and 400 m in the low latitudes is due to the existence of the strong thermocline between 100 and 300 m in the Equatorial Current area. Thus, the two-layer model is considered to be valid only in midlatitudes between 15° and 30°N. The quantitative agreement between the model and observed vertical displacements indicates an important role of the wind stress curl, which induces temperature variation in the subsurface layer.

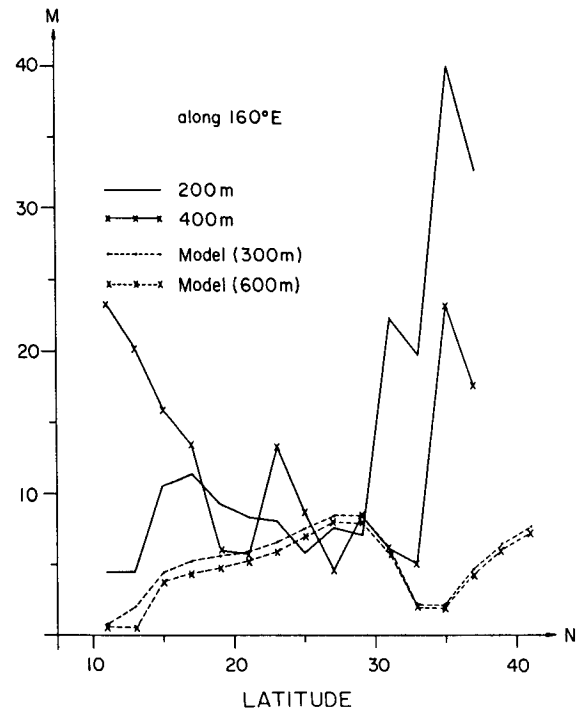

FIG. 8. Amplitude of the seasonal cycle of the main thermocline depth estimated from a two-layer numerical model in cases of interface of 300 m and 600 m in Yoshioka and Yoon (1989). The continuous line is the vertical displacement of isotherms at 200 m and the line with cross at 400 m.

6. Interannual variability of temperature

Interannual temperature data were prepared by subtracting long-term bimonthly means from the bimonthly sequential data and then by filtering out seasonal signals contained in the demeaned data. The low-pass filter employed was a Lanczos taper type with half-power at 0.063 cycles per month (cpm) and 10% at 0.107 cpm. Before applying the filter to the demeaned time sequences, missing data in each time series were interpolated by the cubic spline method, provided that the number of data in the series exceeded 80% of the 120 bimonths.

The RMSD of the low-passed temperature is contoured in Fig. 9. Although the seasonal variability, maximum at the sea surface, diminishes with depth, the magnitude of interannual variability is of the same order at the three different depths so that the ratio of the interannual variability to the seasonal one increases with depth. For example, the ratio in midlatitudes is O(0.1) at the sea surface and O(10) at both 200 and 400 m. This means that the variability at 0 m is mostly seasonal, whereas the variability at deeper depths results from interannual change.

The interannual RMSD temperature at the sea surface is 0.2–0.4°C south of 30°N and increases rapidly with latitudes in the area north of 30°N. At 200 m, low variability less than 1°C lies in a zonal band between 15° and 35°N. The zonal minimum also exists at 100 and 300 m over a wider area, but disappears at 400 m. The disappearance means that the large interannual variability in low latitudes is confined to the depth 100–300 m.

7. Complex empirical orthogonal analysis of interannual variation

To describe the interannual variability of temperature, the complex empirical orthogonal function (CEOF) analysis (e.g., Barnett 1983) was applied to the temperature anomaly at 200 m since it has a representative spatial pattern of the upper ocean involving the anticyclonic circulation and the Equatorial Current. The lowest three CEOF modes explains about 55% of the total variance of the anomalous temperature: the first mode 25.6%, the second 16.6%, and the third 12.6%. Figure 10 is the spatial pattern of amplitude and phase of the first mode. The first mode, having a maximum amplitude along 13°N, suggests important variability in the tropical area south of 20°N, while the second mode (not shown here) may explain the large variability north of the Kuroshio Extension.

The phase map of the first mode shows that there is a sharp change in phase, marked by a dense distribution of isolines east of Japan. The phase inside the area

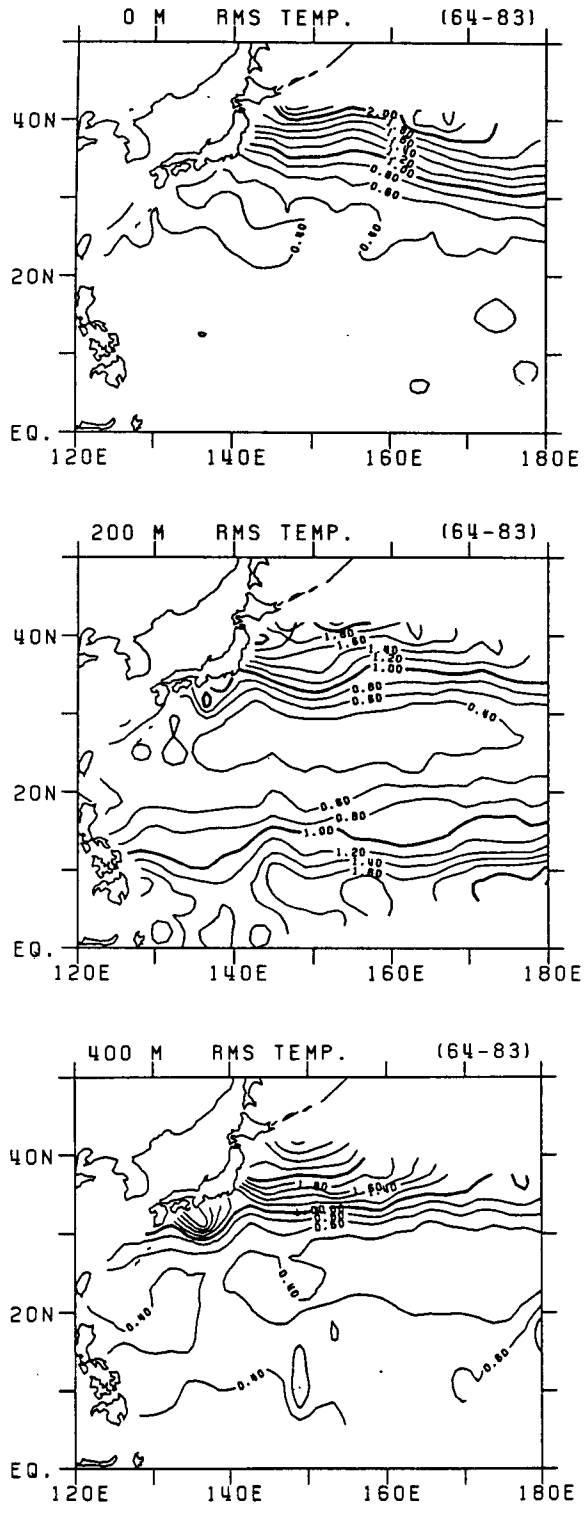

FIG. 9. Root-mean-square temperature of interannual temperature anomaly at the sea surface, 200 m, and 400 m.

surrounded by the dense isolines is larger than 90 degrees, lagging the phase just outside the area by about 180 degrees, though the amplitude is about one-third of that in the tropical area. The phase distribution of the CEOF offers good information on the existence of traveling waves. If progressive waves exist in Fig. 10, the propagating direction corresponds to a direction in which phase decreases. In the southeastern part of the study area the phase decreases gradually, which indicates the existence of waves propagating toward the northwest. Provided that the phase pattern is maintained in the eastern tropical Pacific, the zonal and meridional wavelengths are estimated to be about 15 000 km and 7000 km in the tropical area, respectively. The phase pattern in the small portion of the southwestern study area also presents waves traveling toward the northeast.

Referring to the time function of phase in Fig. 10, the first mode shows a dominant wave period of about 3–4 years. White et al. (1987) have also suggested the same periodicity by analyzing model dynamic height of 22 years and dynamic height observed during 1980–82. Taking the dominant period of 3.5 years, the zonal and meridional phase speeds in the tropical area are approximately 12 and 6 cm s^{-1}, respectively. The spatial maps of the second and third modes do not show evidence of traveling waves. The time function of amplitude for the first mode is maximum in 1969, 1971, 1973, 1976, and 1977. Of these years 1969, 1973, and 1977 correspond to ENSO years. In this figure the 1982–83 ENSO event cannot be identified because of the data truncation by a convolution filter for the CEOF analysis. In addition, the time function of phase shows not only that the phase is nearly 180 degrees when the amplitude in the three ENSO years is maximum but also that the phase after one year of the ENSO year is out of phase with that at the maximum amplitude.

8. Summary and discussions

Long-term seasonal and interannual variability in temperature of the upper ocean over the Northwest Pacific was analyzed using bathythermograph data collected during the 20-year period 1964–83. Data analysis has showed that the temporal variability of temperature is primarily seasonal at the sea surface and interannual at deeper depths below 100 m.

Seasonal variability was found to be most important at the sea surface. It increases with latitude, but decreases rapidly with increasing depth. SST has a very sharp change in seasonal variability in the zonal band between 20° and 30°N, whereas the variability at depths of 200 m is minimal in this zonal band, where the center of the anticyclonic gyre is located. The phase maps of the seasonal cycle of temperature indicated that SST responded directly to surface cooling and warming. The phase of the seasonal cycle at deeper depths led that of SST north to the Kuroshio and Extension, but lagged that south of the Kuroshio and Extension, indicating a phase difference of about 180 degrees between the two areas.

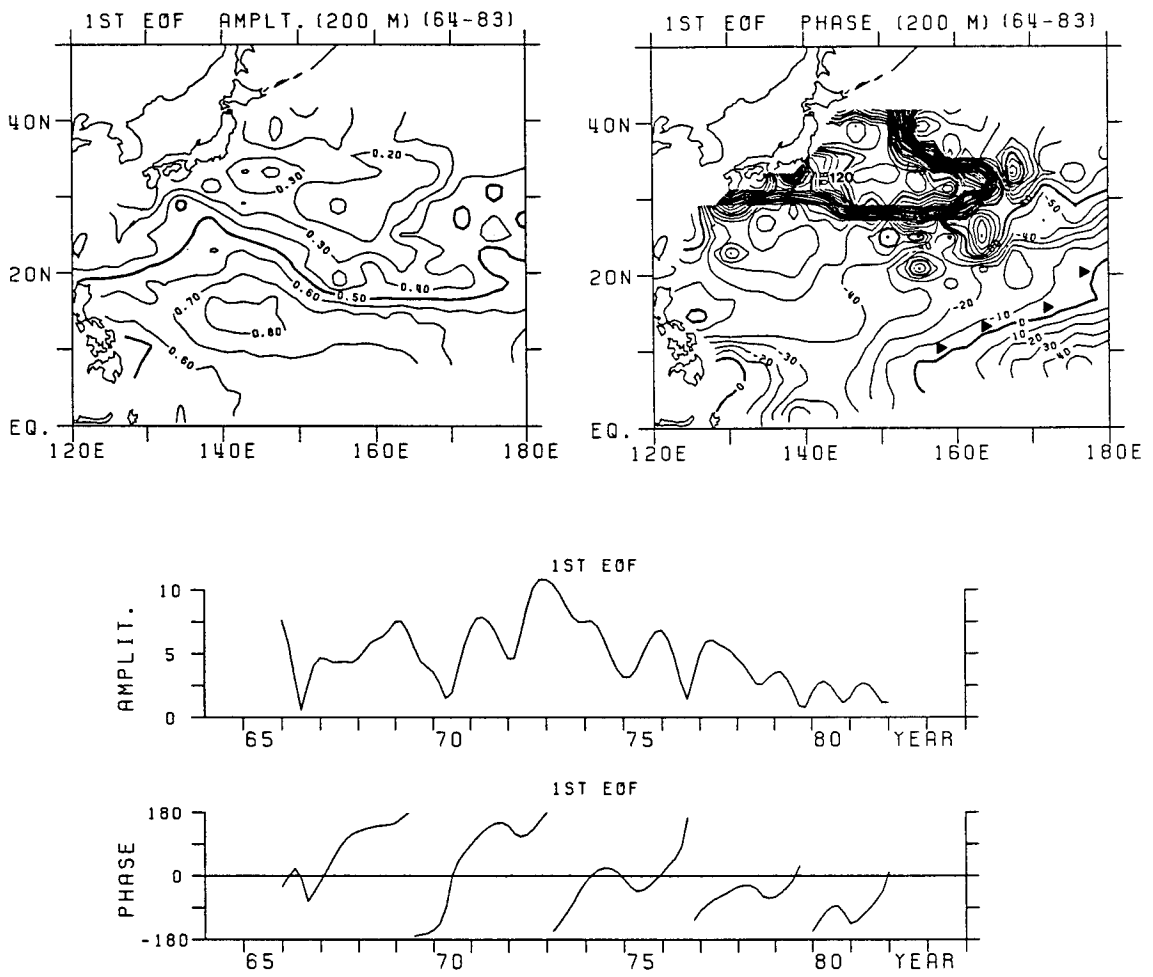

FIG. 10. Spatial pattern of amplitude and phase of the first complex empirical orthogonal function with time functions over the study area.

The zonal minimum of the seasonal variability at depths of 100–300 m seems to be closely associated with wind stress curl over the study area. The mean field of the wind stress curl is negative over the zonal band and positive in low and high latitudes (Kutsuwada 1982) and the curl has a strong seasonal variation (Kutsuwada and Teramoto 1987). The model and observations show that the phase distribution in the northwest Pacific north of a transition line located along 30°–35°N is out of phase with that south of the transition line. The model amplitude of the seasonal cycle of the thermocline depth agrees well with the observed isotherm displacement in area between 15° and 30°N though the model underestimated the amplitude in high and low latitudes.

The largest interannual variability was found at the 200 m depth. The zonal minimum of RMSD at 100 m–300 m between 20°–30°N was not observed at 400 m. The large variability in high latitudes is not directly influenced by the anomaly due to ENSO or tropical disturbances because of the presence of the zonal minimum of RMSD in the 20°–30°N band south of the Kuroshio/Extension. The variability may be related to interannual variation of the atmosphere. The large variability in the tropical Pacific is apparently related to the ENSO disturbances, which is clearly shown in the CEOF analysis.

CEOF analysis of temperature anomaly over the northwest Pacific showed that the first mode, explaining 25% of total variance, had an amplitude several times larger in low latitudes than in high latitudes and it also indicated the existence of an important anomaly during the 1968/69, 1972/73, and 1976/77 winters. When CEOF analysis is applied to the tropical area south of 20°N, the lowest three modes can explain more than 71% of the variance, and the first mode, accounting for 44.5% of the variance, has the same spatial pattern and time functions. The first mode has a dominant period of about 3.5 years and its time function of phase has the same phase of 180 degrees in 1968/69, 1972/73, and 1976/77 winter, corresponding to the ENSO winter. There exist waves propagating northwestward

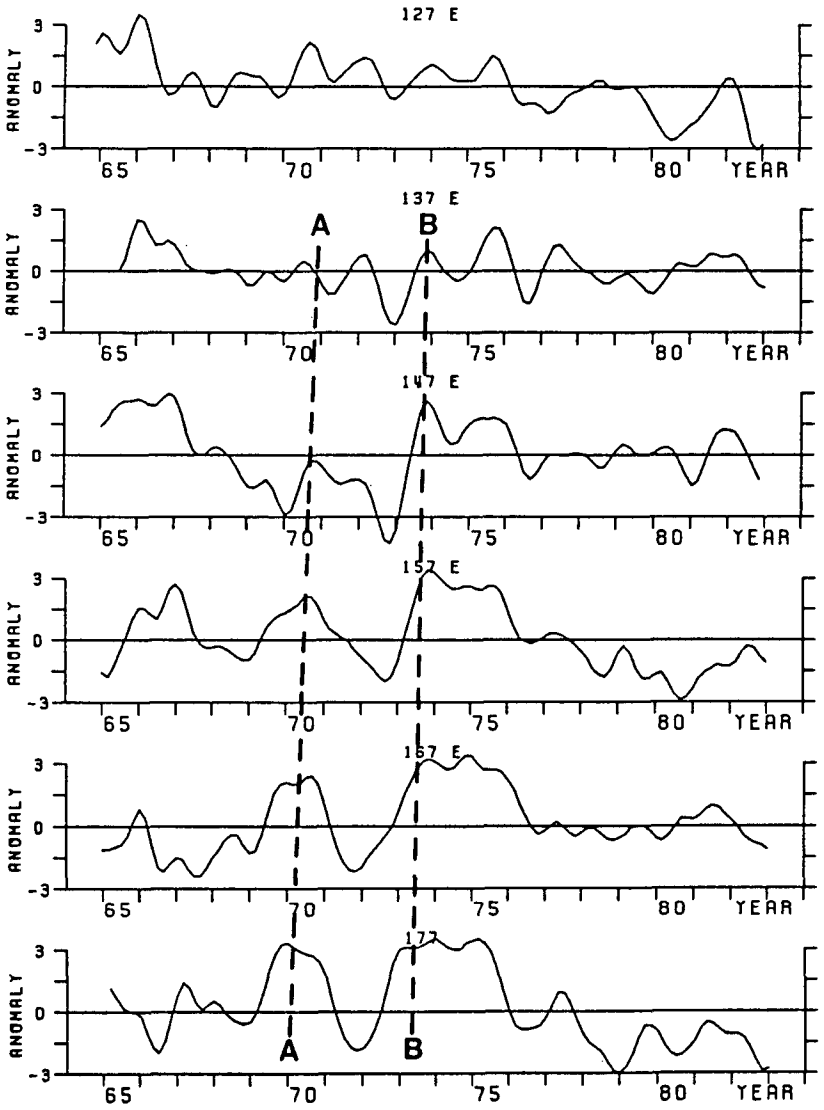

FIG. 11. Time series of interannual temperature anomaly at 200 m along the line 11°N. Lines A and B suggest a westward propagation of positive anomaly.

with a phase speed of 10 cm s^{-1} in the tropical area. The phase speed can be also detected in time series of temperature anomaly. Figure 11 presents the time series of temperature anomaly at the depth of 200 m along 11°N, which shows a westward traveling wave of about 11 cm s^{-1} between 147° and 177°E during 1969–1974.

Acknowledgments. The authors would like to thank deeply Dr. K. Shuto and Dr. Y. Kitamura, the Meteorological Research Institute of Japan, for providing vertical and horizontal maps of temperature calculated from the Levitus dataset, and for assistance in programming, respectively. Special thanks are extended to Dr. K. Mizuno for providing the Far Sea Fisheries' BT dataset. This study was funded by the Korean and Japanese Ministries of Science and Technology. The first author's visit to the Meteorological Research Institute of Japan was supported by the Japanese Ministry.

REFERENCES

Barnett, T. P., 1983: Interaction of the monsoon and Pacific trade wind system at interannual time scales. Part I: The equatorial zone. *Mon. Wea. Rev.*, **111**, 756–773.

Davis, R. E., 1976: Predictability of sea surface temperature and sea level pressure anomalies over the North Pacific Ocean. *J. Phys. Oceanogr.*, **6**, 249–266.

Davis, P. J., and I. Polonsky, 1970: Numerical interpolation, differentiation and integration. *Handbook of Mathematical Functions*, M. Abramowitz, and I. A. Stegun, Eds., Dover, 875–924.

Hanawa, K., T. Watanabe, N. Iwasaka, T. Suga and Y. Toba, 1988: Surface thermal conditions in the western North Pacific. *J. Meteor. Soc. Japan*, **66**, 445–456.

Kutsuwada, K., 1982: New computation of the wind stress over the North Pacific Ocean. *J. Oceanogr. Soc. Japan,* **38,** 159–171.

——, and T. Teramoto, 1987: Monthly maps of surface wind stress field over the North Pacific during 1961–1984. Bull. Ocean Res. Inst. Univ. Tokyo, ISSN 0564-6898, 100 pp.

Levitus, S., 1982: *Climatological Atlas of the World Ocean.* NOAA Prof. Paper No. 13, U.S. Govt. Printing Office, 173 pp.

——, 1987: A comparison of the annual cycle of two sea surface temperature climatologies of the world ocean. *J. Phys. Oceanogr.,* **17,** 197–214.

Nagasaka, K., 1983: Climatology of sea surface temperature in the western North Pacific from 1951 through 1980. *Oceanogr. Mag.,* **33,** 27–42.

Shuto, K., 1989: Seasonal mean distribution of sea properties in the Pacific. Tech. Rep. No. 25, Meteorol. Res. Inst. Japan, 472 pp.

Veronis, G., and H. Stommel, 1956: The action of variable wind stress on a stratified ocean. *J. Mar. Res.,* **15,** 43–75.

Weare, B. C., A. R. Navato and R. E. Newell, 1976: Empirical orthogonal analysis of Pacific sea surface temperature. *J. Phys. Oceanogr.,* **6,** 671–678.

White, W. B., 1978: A wind-driven model experiment of the seasonal cycle of the main thermocline in the interior midlatitude North Pacific. *J. Phys. Oceanogr.,* **8,** 818–824.

——, and K. Hasunuma, 1980: Large-scale interannual variability in the baroclinic gyre structure of the western North Pacific from 1954–1974. *J. Mar. Res.,* **38,** 651–672.

——, and R. L. Bernstein, 1979: Design of an oceanographic network in the midlatitude North Pacific. *J. Phys. Oceanogr.,* **9,** 592–606.

——, G. A. Meyers, J. R. Donguy and S. E. Pazan, 1985a: Short-term climatic variability in the thermal structure of the Pacific Ocean during 1979–82. *J. Phys. Oceanogr.,* **5,** 917–935.

——, S. E. Pazan and B. Li, 1985b: Processes of short-term climatic variability in the baroclinic structure of the interior western tropical North Pacific. *J. Phys. Oceanogr.,* **15,** 386–402.

——, ——, and M. Inoue, 1987: Hindcast/forecast of ENSO events based upon the redistribution of observed and model heat content in the western tropical Pacific, 1964–86. *J. Phys. Oceanogr.,* **17,** 264–280.

Yoshioka, N., and J. W. Yoon, 1989: Variations in the North Pacific subtropical circulation found in a quasi-geostrophic model driven by observed wind fields. *J. Oceanogr. Soc. Japan,* submitted.